Valence-band structures of layered oxychalcogenides, LaCuOCh (Ch=S, Se, and Te), studied by ultraviolet photoemission spectroscopy and energy-band calculations

doi: 10.1063/1.2001749

Valence-band structures of layered oxychalcogenides, LaCuOCh (Ch=S, Se, and Te), studied by ultraviolet photoemission spectroscopy and energy-band calculations

Kazushige Ueda[a)]
Department of Materials Science, Faculty of Engineering, Kyushu Institute of Technology, 1-1 Sensui, Tobata, Kitakyushu 804-8550, Japan and Solution-Oriented Study for Science and Technology (SORST), Japan Science and Technology Agency, Kawaguchi Center Building, 4-1-8 Honcho, Kawaguchi-shi, Saitama 332-0012, Japan

Hideo Hosono
Frontier Collaborative Research Center, Tokyo Institute of Technology, 4259 Nagatsuta, Midori, Yokohama 226-8503, Japan and Solution-Oriented Study for Science and Technology (SORST), Japan Science and Technology Agency, Kawaguchi Center Building, 4-1-8 Honcho, Kawaguchi-shi, Saitama 332-0012, Japan

Noriaki Hamada
Department of Physics, Faculty of Science and Technology, Tokyo University of Science, 2641 Yamazaki, Noda, Chiba 278-8510, Japan

(Received 10 May 2005; accepted 28 June 2005; published online 18 August 2005)

To examine the electronic structure of the valence band, ultraviolet photoemission spectra of a series of layered oxychalcogenides, LaCuOCh (Ch=S, Se, and Te), were measured. The measurements were conducted using He II, He I, and Ne I excitation lines to observe the excitation energy dependence of the spectral shape. Energy-band calculations based on a full-potential linearized augmented plain-wave method were performed. The calculated density of states and partial density of states were compared to the observed photoemission spectra. Five bands were observed in the valence band of LaCuOCh, and Ne I radiation remarkably enhanced two of them. The energy dependence of the photoionization cross section of atomic orbitals indicated that the two enhanced bands were due to the Ch *p* states. Energy calculations were used to assign the remaining bands. The electronic structure of LaCuOCh was further discussed using molecular-orbital diagrams to visualize the $(La_2O_2)^{2+}$ and $(Cu_2Ch_2)^{2-}$ layers as large donor-acceptor pairs. The energy-band calculation and molecular-orbital diagram analyses suggested that the main difference among the valence-band structures of LaCuOCh (Ch=S, Se, and Te) originates from the variations in the energy position of the Ch *p* bands. The observed spectra are consistent with the results of the band calculations and clearly show the energy variations in the Ch *p* bands with respect to spectral shape and excitation energy dependence. © *2005 American Institute of Physics*.
[DOI: 10.1063/1.2001749]

I. INTRODUCTION

LaCuOCh (Ch=S, Se, and Te) oxychalcogenides are mixed-anion materials that consist of divalent oxygen and chalcogen anions. In contrast to ordinary oxychalcogenides, O^{2-} ions are only coordinated by La^{3+} ions and Cu^{+} ions are exclusively coordinated by sulfur anions, which form the layered structure shown in Fig. 1.[1] The $(La_2O_2)^{2+}$ oxide layers and $(Cu_2Ch_2)^{2-}$ chalcogenide layers are spatially separated as alternating stacks along the *c* axis that form the layered structure. The sublattice of the $(Cu_2Ch_2)^{2-}$ layers formed from edge-sharing $CuCh_4$ tetrahedra is also found in other layered materials such as $Sr_2Cu_2ZnO_2S_2$,[2] $BaCu_2S_2$,[3] BaCuFS,[4] and ACu_3S_4 (*A*=K, Rb, Cs, and Tl).[5] It was concluded from a study on the electronic structure of the $(Cu_2S_2)^{2-}$ layers in these materials[6–9] that a large hybridization between Cu 3*d* and S 3*p* orbitals occurs in the Cu–S antibonding states at the top of the valence band.

It was proposed that these layered materials can be regarded as compounds formed with donor-acceptor layers, and a similarity exists between this layered structure and multiple quantum wells.[10] These ideas are useful for designing various layered materials with electronic functions. For LaCuOCh (Ch=S, Se, and Te), the $(La_2O_2)^{2+}$ layers correspond to donor layers or potential barriers for carrier confinement and the $(Cu_2Ch_2)^{2-}$ layers to acceptor layers or quantum wells. It is noteworthy that both conduction-band minimum (CBM) and valence-band maximum (VBM) are primarily determined by the $(Cu_2Ch_2)^{2-}$ layers in LaCuOCh. These layered structures lead to a band gap much wider than Cu_2S, *p*-type degenerate conduction, and light-emitting properties due to the RT stable excitons in LaCuOS and LaCuOSe.[11] Moreover, the features of multiple quantum wells are demonstrated in these materials by observing the steplike density of states (DOS) in the absorption spectra[12] of epitaxially grown thin films.[13] These quantum effects are also observed in $La_2CdO_2Se_2$ with $(Cu_2Se_2)^{2-}$ layers.[14] The

[a)]FAX: +81-93-884-3300; electronic mail: kueda@che.kyutech.ac.jp

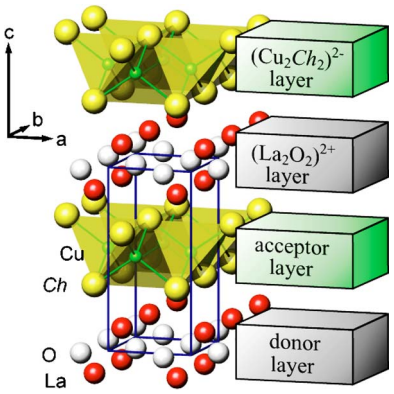

FIG. 1. (Color online) Crystal structure of LaCuOCh (Ch=S, Se, and Te). Alternating stacks of $(La_2O_2)^{2+}$ and $(Cu_2Ch_2)^{2-}$ layers form the layered crystal structure.

value of the band gap in CdSe nanoparticles approaches that in $La_2CdO_2Se_2$ as the size of the nanoparticles decreases. This observation suggests that the $(CdSe_2)^{2-}$ layers in $La_2CdO_2Se_2$ are the extreme two-dimensional end of bulk CdSe embedded in the three-dimentional crystal structure.

The electronic structure of LaCuOS was examined in a previous study using normal/inverse photoemission spectroscopy (PES/IPES) and energy-band calculations.[15] Figure 2 shows the observed and calculated electronic structures of LaCuOS in which several bands were in the CB and VB. Analogous electronic structures were also found in LnCuOS (Ln=La–Nd except for Ce).[16] Recently, energy-band calculations were performed for a series of LaCuOCh (Ch=S, Se, and Te) using a full-potential linearized augmented plain-wave (FLAPW) method.[17] In this study, the PES spectra of LaCuOCh (Ch=S, Se, and Te) were measured using the three types of UV excitation lines and compared to energy-band calculation results. The observed spectra show a conspicuous excitation energy dependence on the Ch *p* bands in these materials and revealed that the VB is composed of not four bands as previously analyzed, but five bands (from *A* to *E*) as shown in Fig. 2.[18] The five-band structures of the VB are assigned with respect to both the PES spectra and the calculated DOS. The electronic structures of a series of LaCuOCh are interpreted in terms of a layered structure and the differences between them are discussed.

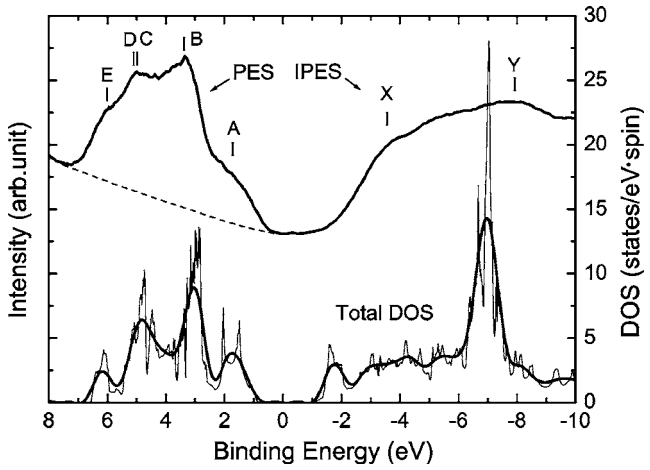

FIG. 2. PES (UPS) and IPES spectra of LaCuOS along with the calculated total DOS. The dashed line is the background of the PES spectrum. The thin line in total DOS indicates the profile in the as-calculated DOS and the thick line denotes the DOS after smearing treatment.

II. EXPERIMENTS

A. Sample preparation

LaCuOS and LaCuOSe were synthesized by conventional solid-state reactions in evacuated silica glass tubes. La_2O_3, La_2S_3, and Cu_2S were used as the starting materials for LaCuOS, while La_2O_3, a La_2Se_3 precursor, Cu, and Se were used for LaCuOSe. The La_2Se_3 precursor was prepared in advance by a solid-state reaction of La with Se at 300° C in an evacuated silica glass tube. The starting materials were stoichiometrically mixed and the mixed powders were heated at 800° C for 6 h in evacuated silica tubes. To prepare LaCuOTe, La, La_2O_3, Cu, and Te were used as starting materials since the La_2Te_3 precursor and La_2O_2Te are unstable and easily oxidize under an ambient atmosphere. Stoichiometric amounts of the starting materials were mixed and initially heated at 300° C for 6 h in an evacuated silica tube to complete the reaction between La, Cu, and Te. Then the product was remixed in the evacuated silica tube by shaking the tube and heated at 800° C for 6 h. X-ray powder diffraction measurements indicated that each sample was a single phase.

B. Ultraviolet photoemission spectroscopy (UPS)

The UPS measurements were conducted using a discharged lamp (VG Scientific) that emitted excitation lines of He II (40.8 eV), He I (21.2 eV), and Ne I (16.7 eV). Highly conductive dense disks are required for spectra with low background noise. Each powder sample was pressed and sintered by a spark plasma sintering system (Sumitomo Coal Mining Co.). Each sintered disk showed an apparent density higher than 90% and electrical conductivity sufficient to prevent charging effects during UPS measurements. The surfaces of the samples were scraped with a diamond file under a vacuum of 8×10^{-10} Torr to obtain clean surfaces before each measurement. The UPS spectra were measured at 5×10^{-8} Torr. The Fermi energy (E_F) of Au was used to calibrate the binding energy (E_B) in each spectrum. In the analysis of the valence-band structure, the background in the UPS spectra, which for example is the dashed line in Fig. 2, was subtracted smoothly. The VBM for each sample is almost at E_F (E_B=0 eV) as shown in Fig. 2 since all the samples were *p*-type conductors. However, the energy of the VBM differed slightly between samples, probably due to the carrier density or the acceptor levels. To compare the UPS spectra with the calculated electronic structure in detail, the VBM in each spectrum was accurately aligned at the binding energy of E_B=0 eV.

C. Energy-band calculations

The energy-band structures of LaCuOCh (Ch=S, Se, and Te) were calculated by the ABCAP code of a FLAPW method.[19] The FLAPW calculations based on density-functional theory were performed using a local-density ap-

TABLE I. Photoionization cross sections of atomic orbitals (Mb/at.) at different UV excitation energies.[a]

Light source (energy)	Cu 3*d*	O 2*p*	S 3*p*	Se 4*p*	Te 5*p*
He II (40.8 eV)	9.944 (1.000)[b]	6.816 (0.6854)	0.6051 (0.060 85)	0.5578 (0.056 09)	0.5043 (0.050 71)
He I (21.2 eV)	7.285 (1.000)[b]	10.69 (1.467)	4.371 (0.6000)	8.057 (1.106)	4.758 (0.6531)
Ne I (16.7 eV)	6.284 (1.000)[b]	10.43 (1.660)	18.25 (2.904)	20.18 (3.211)	11.54 (1.836)

[a]See Ref. 23.
[b]The values in the parentheses are normalized by the value for the Cu 3*d* orbital in each excitation.

proximation (LDA) with an on-site correlation for La 4*f* electrons. The crystal structural parameters were taken from previous papers: Ref. 20 for LaCuOS and LaCuOSe and Ref. 21 for LaCuOTe. Each crystal structure belongs to the tetragonal system with a $P4/nmm$ space group, but the lattice parameters and atomic positions of La and Ch (Ch=S, Se, and Te) slightly differed. The muffin-tin radii used in the calculations were 2.7 a.u. for La, 2.1 a.u. for Cu, 1.4 a.u. for O, 1.9 a.u. for S, 2.0 a.u. for Se, and 2.5 a.u. for Te. The calculations were self-consistently iterated until the total electron energy of the crystals converged into less than 0.1 mRy. The total DOS and partial DOS (PDOS) were calculated with the tetrahedron method. In the ABCAP code, the total DOS refers to all energy states in space, but the PDOS only refers to energy states within the muffin-tin spheres. However, more than 70% of the total DOS are covered by the PDOS in the occupied states. In the analysis of the valence-band structure, the origin of the energy scale in the calculated DOS and PDOS was the VBM. Moreover, a smearing treatment, which is shown as the thick line in Fig. 2, was added to the DOS/PDOS in order to compare the DOS/PDOS with the UPS spectra.

III. RESULTS AND DISCUSSION

A. Photoionization cross section

The photoemission process includes photoionization of atoms or ions at the surface and near-surface regions of compounds.[22] Although the atoms in compounds form chemical bonds with each other, the intensity of the photoemission spectra usually depends on the photoionization probability of the atoms. Therefore, the data on the photoionization cross sections of the atomic orbitals are indispensable when considering the shape of the photoemission spectra. Before discussing the obtained photoemission spectra, the photoionization cross sections of atomic orbitals relevant to the electronic structure of LaCuOCh (Ch=S, Se, and Te) are evaluated.

Our previous study indicated that the valence bands of LaCuOCh (Ch=S, Se, and Te) are primarily composed of Cu 3*d*, O 2*p*, and Ch *p* orbitals.[15,17] Table I lists the photoionization cross sections of these atomic orbitals at each excitation energy.[23] The photoionization cross section of the Cu 3*d* orbital slightly decreases, while that of the O 2*p* orbital gradually increases as the excitation energy decreases. The values of these cross sections vary within the same order of magnitude, but the variations against the excitation energy for these two orbitals are relatively small. On the other hand, the cross sections of the Ch *p* orbitals (S 3*p*, Se 4*p*, and Te 5*p* orbitals) are strongly enhanced as the excitation energy decreases. The values of the cross sections increase by an order of magnitude from the excitation by He II to He I, and further increase almost three to four times from He I to Ne I. This large excitation energy dependence of the cross sections in the Ch *p* orbitals is considerably different from those in the Cu 3*d* and O 2*p* orbitals.

These features in the photoionization cross sections are useful for understanding the obtained photoemission spectra and are helpful for assigning the components of the valence-band structure. However, comparing the intensities in the UPS spectra is usually difficult since the intensities measured using different excitation lines do not correlate. Therefore, the intensities of the obtained UPS spectra were normalized using the energy position of the Cu 3*d* nonbonding band. As reported in previous papers[15,17] and discussed below, the energy position of the Cu 3*d* nonbonding band is located at the energy where the PDOS of the Cu 3*d* states is maximized. Since the total DOS at this energy is almost exclusively derived from the PDOS of the Cu 3*d* states and the Cu 3*d* photoionization cross section only slightly depends on the excitation energy, normalization of the intensities by the Cu 3*d* nonbonding band is reasonable for comparing the UPS spectra measured using different excitation energies.

B. LaCuOS

Figure 3(a) shows the UPS spectra of LaCuOS measured using the excitation lines of He II, He I, and Ne I along with the total DOS and PDOS of Cu 3*d*, O 2*p*, and S 3*p* states. In Fig. 3(a), the binding energy for the UPS spectra (upper *x* axis) is shifted against the energy for the DOS/PDOS (bottom *x* axis) to compare the shape of the spectra. The intensities of the UPS spectra are normalized at a binding energy where the PDOS of Cu 3*d* states is maximized, approximately 3 eV. Four bands, which are roughly assigned from the VBM in our previous study as Cu 3*d*–S 3*p* hybridized band, Cu 3*d* band, S 3*p* band, and O 2*p* band, are resolved in the UPS spectra. However, the present study revealed that the previous assignment is inaccurate and five bands actually explain the shape of the UPS spectra for LaCuOCh (Ch=S, Se, and Te). The five bands, shown in Fig. 3(a), are indexed

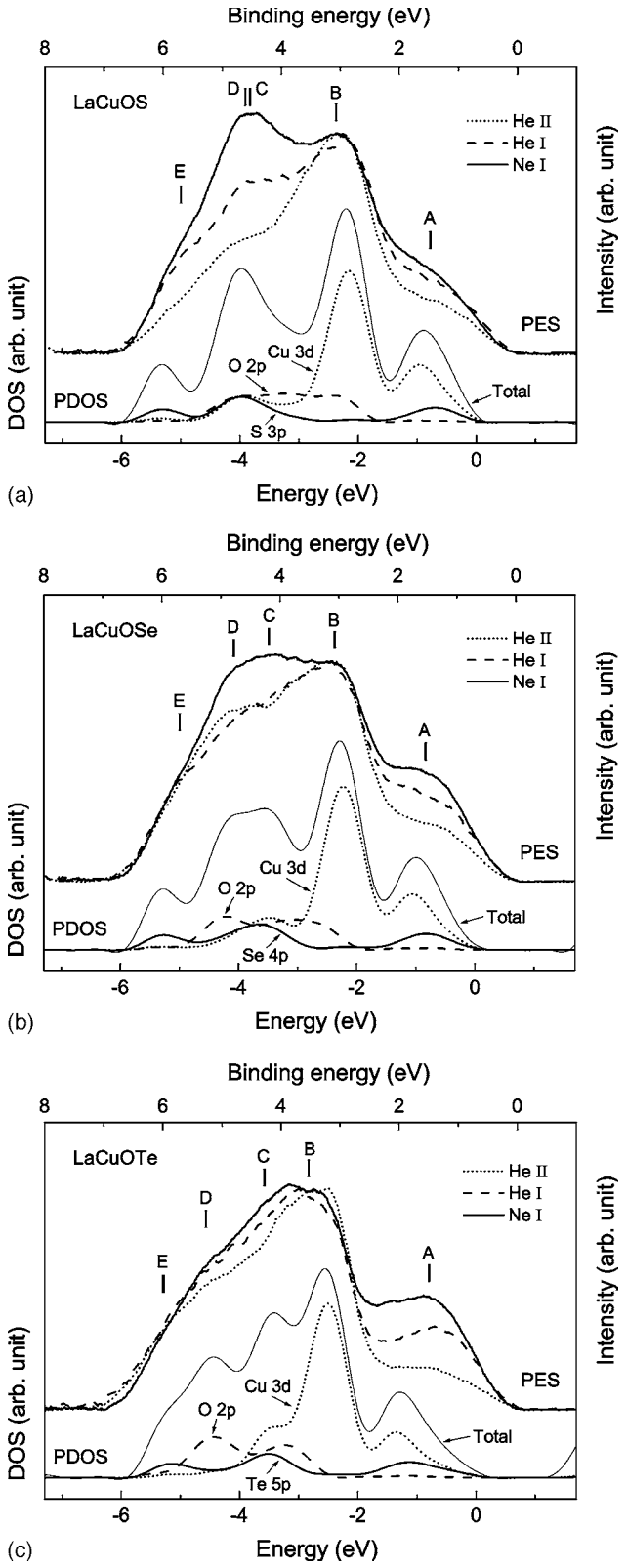

FIG. 3. UPS spectra obtained by three excitation lines (He II, He I, and Ne I) for (a) LaCuOS, (b) LaCuOSe, and (c) LaCuOTe. The total and partial DOSs (Cu 3*d*, O 2*p*, and Ch *p* states) are shown under the PES spectra.

as bands *A* to *E* from the VBM. Bands *C* and *D* happen to be located at almost the same energy in LaCuOS.

Band *A* is right below the VBM and its intensity increases as the excitation energy decreases. This excitation energy dependence suggests that band *A* includes components from the S 3*p* states. Since the calculated PDOSs show that band *A* is mainly composed of the Cu 3*d* and S 3*p* states, band *A* is assigned to a Cu 3*d*–S 3*p* antibonding band. Band *B* is located at a binding energy of approximately 3.0 eV, which is due to the Cu 3*d* nonbonding band since the PDOS maximum of the Cu 3*d* states is also located at this energy. Band *C* is assigned to the S 3*p*–Cu 3*d* bonding band, which forms the counterpart to band *A*. The intensity of band *C* is strongly enhanced as the excitation energy decreases and corresponds to the increase in the photoionization cross section of the S 3*p* orbitals. The PDOSs of S 3*p* and Cu 3*d* states show overlapped bands at the energy for band *C*. A broad band indexed as *D* is at the same energy as band *C* in the UPS spectrum of He II. Since the photoionization cross section of the S 3*p* orbitals is negligible in the He II radiation, the PDOS of the O 2*p* states indicates that band *D* is an O 2*p* band. The energy range of the PDOS of the O 2*p* states is from −2 to −5 eV in LaCuOCh (Ch=S, Se, and Te) and consists of two components: the O 2*p*–La 5*d* bonding band in the lower energy region and the O 2*p* nonbonding band in the higher energy region. Since the PDOS of La 5*d* states appears at the same energy for band *D* as shown in the previous study,[15,17] band *D* is assigned to the O 2*p*–La 5*d* bonding band. However, the O 2*p* states are dominant in band *D* because the PDOS of the La 5*d* states is much smaller than that of the O 2*p* states.[15,17] Band *E* is located at the bottom of the VB. Band *E* intensities increase as the excitation energy decreases and noticeable S 3*p* states seen in the PDOS correspond to band *E*. Although it is unclear in Fig. 3(a) due to the smearing treatment, the Cu 4*s* and 3*d* states and the S 3*p* states are clearly observed in the energy for band *E* in the previous study.[15,17] Therefore, band *E* is assigned to the S 3*p*–Cu 4*s*, 3*d* bonding bands.

C. LaCuOSe

Figure 3(b) shows the UPS spectra of LaCuOSe along with the total DOS and PDOSs. Five bands from *A* to *E* are indexed in a similar manner as LaCuOS. Bands *A* to *E* are assigned to the Se 4*p*–Cu 3*d* antibonding band, Cu 3*d* nonbonding band, Se 4*p*–Cu 3*d* bonding band, O 2*p*–La 5*d* bonding band, and Se 4*p*–Cu 4*s*, 3*d* bonding bands, respectively.

As shown in the PDOSs, the Se 4*p* states are included in bands *A*, *C*, and *E*. The intensity of band *A* is enhanced as the excitation energy decreases and the enhancement in LaCuOSe is larger than that in LaCuOS. This larger enhancement suggests that Se 4*p* and Cu 3*d* states are more hybridized and the amount of the Se 4*p* states increases in band *A*. The enhancement of band *C* is also seen in the Ne I UPS spectrum. The energy for band *C* is shallower than that found in LaCuOS, and bands *C* and *D* show broad features in the middle of the VB. Band *D* becomes clear in the He II UPS spectrum. These observations are supported by the calculated DOS and PDOS. In contrast to LaCuOS, bands *C* and *D* split in LaCuOSe, giving a broad band between bands *B* and *E*. Excitation energy dependence is not seen for band *E* in the UPS spectra despite that band *E* includes the Se 4*p* states, which is probably due to the bonding feature of band

E. The total amount of PDOSs for Se 4*p*, Cu 4*s*, and 3*d* are smaller in band *E* than in band *A*. This small amount of PDOSs indicates that most of the Se and Cu states are located outside of the muffin-tin spheres and bonding states are formed in the interatomic region between Se and Cu ions. Since these bonding states are not simply described by atomic orbitals, the photoionization cross sections of atomic orbitals are invalid for these bonding states. Therefore, unlike bands *A* and *C*, the intensity of band *E* does not show an obvious excitation energy dependence.

D. LaCuOTe

Figure 3(c) shows the UPS spectra of LaCuOTe and its DOS/PDOSs. Except for the band near the VBM, the UPS spectra of LaCuOTe are less structured than LaCuOS and LaCuOSe, but five bands from *A* to *E* are indexed using the calculated PDOS. The five bands, *A* to *E*, are assigned to the Te 5*p*–Cu 3*d* antibonding band, Cu 3*d* nonbonding band, Te 5*p*–Cu 3*d* bonding band, O 2*p*–La 5*d* bonding band, and Te 5*p*–Cu 4*s*, 3*d* bonding bands, respectively.

The intensity of band *A* is remarkably enhanced as the excitation energy decreases. Since this enhancement is the largest among LaCuOCh, band *A* includes a large amount of Te 5*p* states due to the large hybridization between the Te 5*p* and Cu 3*d* states. The intensity of band *C* increases as the excitation energy decreases and the splitting of bands *C* and *D* in LaCuOTe is larger than that in LaCuOSe. Band *E* in LaCuOTe does not show an excitation energy dependence for the same reasons as discussed for LaCuOSe.

It is noteworthy that, in the Ne I UPS spectrum, the enhancement of band *C* for LaCuOTe is relatively small compared to LaCuOS and LaCuOSe, which contrasts the large excitation energy dependence of band *A* in LaCuOTe. When the degree of the enhancement in bands *A* and *C* is compared in a series of LaCuOCh, band *C* is enhanced more than band *A* in LaCuOS, while bands *A* and *C* are similarly enhanced in LaCuOSe, but in LaCuOTe band *A* is enhanced more than band *C*. Namely, it seems that the enhancement gradually moves from the deep *C* band to the shallow *A* band as the chalcogen ions change from S to Te. Since the enhancement in the Ne I spectra results from Ch *p* states, the shift of the enhancement from band *C* to *A* suggests that there is variation in the amount of Ch *p* states within the two Ch *p*–Cu 3*d* hybridized bands *A* and *C*. Although the PDOS does not clearly support this idea, the shallow shift of the band enhancement probably originates from the energy levels of the Ch *p* atomic orbitals; −10.3 eV for S 3*p*, −9.5 eV for Se 4*p*, and −8.6 eV for Te 5*p* against −10.1 eV for Cu 3*d* orbials.[23]

E. Comparing valance-band structures between LaCuOCh (Ch=S, Se, and Te)

Figure 4 shows the He I UPS spectra and the total DOSs for LaCuOCh (Ch=S, Se, and Te) to compare the differences in their valence-band structure. Band *A* is assigned to the Ch *p*–Cu 3*d* antibond band. The peak that corresponds to this band in total DOS moves to a higher binding energy, which is inconsistent with the UPS spectra. However, the width of band *A* becomes larger in both the UPS spectra and total

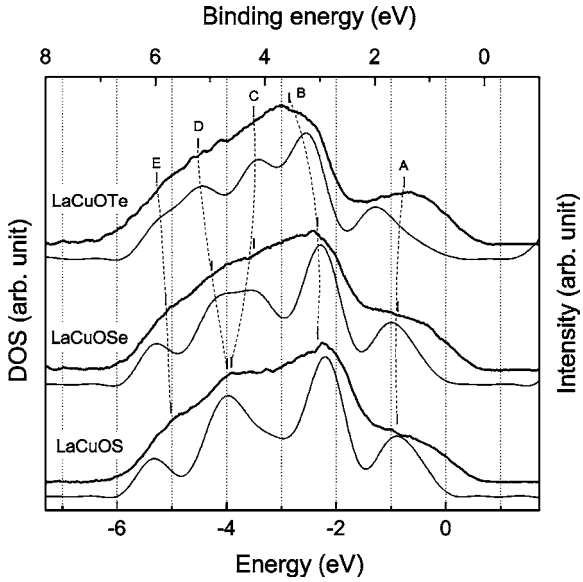

FIG. 4. He I UPS spectra and total DOSs of LaCuOCh (Ch=S, Se, and Te).

DOS in the order of LaCuOS, LaCuOSe, and LaCuOTe, suggesting that the hybridization between Ch *p* and Cu 3*d* increases in the same order. Band *B* is assigned to the Cu 3*d* nonbonding band. The shape of band *B* is very similar among LaCuOCh, but the energy position shifts slightly deeper in the binding energy from LaCuOS to LaCuOTe. Bands *C* and *D* are assigned to the Ch *p*–Cu 3*d* and the O 2*p*–La 5*d* bonding bands, respectively. These two bands are at the same energy in LaCuOS and are separate in LaCuOSe and LaCuOTe since band *C* shifts to a smaller binding energy while band *D* goes to a larger binding energy. The separation between bands *C* and *D* in LaCuOTe is larger than that in LaCuOSe. This shift of band *C* to a smaller binding energy is derived from the atomic energy level of the Ch *p* orbitals. Band *E* is located at the bottom of the valence band and significant differences were not observed between LaCuOCh.

To further understand the valence-band structure of LaCuOCh, the electronic states of each layer were examined. As shown in Fig. 1, the crystal structure of LaCuOCh is composed of $(La_2O_2)^{2+}$ and $(Cu_2Ch_2)^{2-}$ layers. Since the La–Ch distance is much larger than the simple ionic radii, interactions between La and Ch ions are weak.[20] Accordingly, it can be approximated that these layers only interact electrostatically and are alternating stacks along the *c* axis. Thus, covalent bonding is negligible between the layers. Namely, these two layers may be treated like isolated charged layers; the $(La_2O_2)^{2+}$ layers act as donor layers and $(Cu_2Ch_2)^{2-}$ layers act as acceptor layers. Therefore, the valence-band structure of LaCuOCh is interpreted by the superposition of the bands formed in each of $(La_2O_2)^{2+}$ and $(Cu_2Ch_2)^{2-}$ layers.

Figure 5 shows schematic molecular-orbital diagrams of the $(La_2O_2)^{2+}$ and $(Cu_2Ch_2)^{2-}$ layers. The $(La_2O_2)^{2+}$ layers are composed of La and O atoms, and the energy levels of these atomic orbitals are considerably different as shown in the left side of the figure. Therefore, the chemical bonds between these atoms are ionic and the occupied band in the

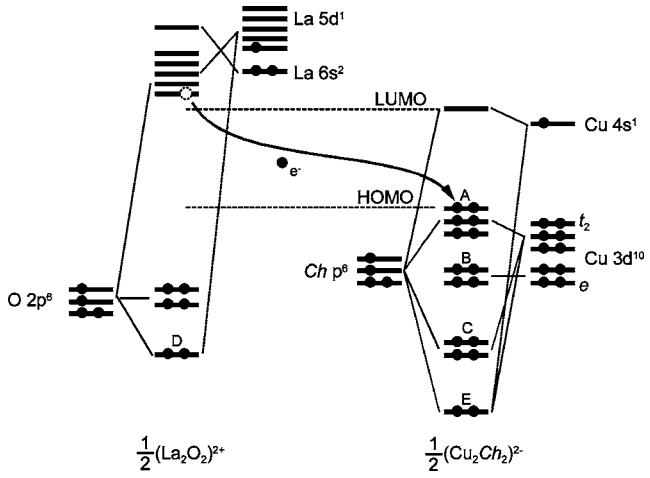

FIG. 5. Schematic molecular-orbital diagrams of LaCuOCh (Ch=S, Se, and Te) that consists of $(La_2O_2)^{2+}$ and $(Cu_2Ch_2)^{2-}$ layers. Each diagram is shown in a half unit of the layers.

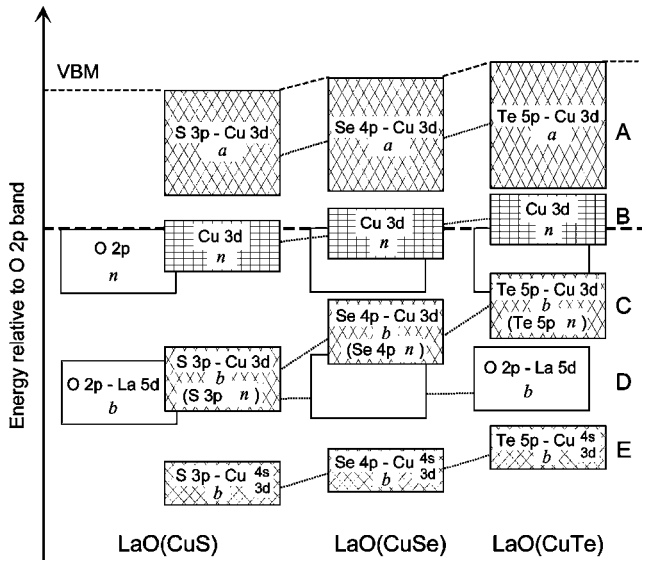

FIG. 6. Schematic energy-band structures of LaCuOCh (Ch=S, Se, and Te) aligned with the energy level of the O 2*p* nonbonding band. The symbols *b*, *n*, and *a* denote bonding, nonbonding, and antibonding orbitals, respectively.

$(La_2O_2)^{2+}$ layers is mainly composed of O 2*p* orbitals. The lone-pair-like feature of the electrons in the O ions remains due to the strong electronegative nature of oxygen. Accordingly, the O 2*p* occupied band consists of two bands, the O 2*p*–La 5*d* bonding band and the O 2*p* nonbonding band. Since the bonding band is energetically stabilized, the O 2*p*–La 5*d* bonding band, which corresponds to band *D*, is below the O 2*p* nonbonding band. The excessive electrons in the $(La_2O_2)^{2+}$ layers are transferred to the $(Cu_2Ch_2)^{2-}$ layers.

The two bands, O 2*p*–La 5*d* bonding band and O 2*p* nonbonding band, are clearly observed in the PDOS of the O 2*p* states for LaCuOSe and LaCuOTe in Figs. 3(b) and 3(c), respectively. The PDOS of the O 2*p* nonbonding band overlaps that of the Cu 3*d* states and the O 2*p* nonbonding band has a negligible influence on the shape of the UPS spectra. Therefore, the existence of the O 2*p* nonbonding band was neglected in the discussion above. However, the nonbonding feature of the O 2*p* states is convenient when considering the relative energy scale between LaCuOCh as shown later.

The crystal structure of the $(Cu_2Ch_2)^{2-}$ layers are the same as those of the $(Cu_2S_2)^{2-}$ layers in the ACu_2S_2 (A =Ba and Tl) and $(Mn_2P_2)^{2-}$ layers in $BaMn_2P_2$. These compounds crystallize in a $ThCr_2Si_2$-type structure and their electronic structures were previously reported.[7,9] Referring to these previous reports, the electronic structure of the $(Cu_2Ch_2)^{2-}$ layer is interpreted in a similar manner. Atomic Cu 3*d* degenerate states split into t_2 and *e* states under a tetrahedral crystal field where the t_2 states are above the *e* states. The Cu 3*d e* states are Cu 3*d* nonbonding states that do not interact with the Ch *p* states. These Cu 3*d* nonbonding states correspond to band *B*. The Cu 3*d* t_2 states and the Ch *p* states interact to form bonding and antibonding states, which correspond to bands *C* and *A*, respectively. These antibonding states correspond to the highest occupied molecular rotbital (HOMO) in the $(Cu_2Ch_2)^{2-}$ layer and form the VBM in LaCuOCh. Since the Ch ions are at the apex of the square pyramid of Cu ions, the lone-pair or nonbonding states of Ch *p* exist and are mainly in band *C*. The Cu 4*s* state interacts with the Ch *p* states to form the bonding state, which is assigned to band *E*, which also contains the Cu 3*d* t_2–Ch *p* bonding states. The antibonding state between Cu 4*s* and Ch *p* states is formed as the lowest unoccupied molecular orbital (LUMO), which becomes the CBM in LaCuOS and LaCuOSe.

Since the electronic states of each layer are understood as shown in Fig. 5, the energy-band structure of LaCuOCh is interpreted by superposing the energy bands of the two layers. Considering the relative energies of these energy bands from the UPS spectra and PDOSs, Fig. 6 schematically summarizes the valence-band structures of a series of LaCuOCh. Since the other ions barely influence the energy level of the O 2*p* nonbonding band, the energy levels of the bands in LaCuOCh were aligned at the edge of the O 2*p* nonbonding band obtained in the PDOS calculations. This alignment using the O 2*p* nonbonding band is more reasonable than the alignment at the VBM as shown in Fig. 4 when the energy is scaled from the vacuum level. In Fig. 6, the most notable difference between LaCuOCh is the energy of the Ch *p*–Cu 3*d* bonding band (band *C*). This band has a larger energy shift than the other bands. The energy of the VBM also becomes shallower in the order of LaCuOS, LaCuOSe, and LaCuOTe, which is consistent with the fact that the band gap of LaCuOCh becomes smaller in the same order.[17]

Examining the valence-band structure in a series of LaCuOCh revealed that the variation of the energy levels of the Ch *p* states in LaCuOCh is responsible for the different shapes in the UPS spectra. The shallower shift of the Ch *p* states simultaneously changed the degree of hybridization between the Ch *p* and Cu 3*d* states in bands *A* and *C*. This feature was observed in the UPS spectra measured using different excitation energy.

IV. CONCLUSION

The UPS spectra of LaCuOCh (Ch=S, Se, and Te) were measured using the excitation lines of He II, He I, and Ne I and examined using the photoionization cross section of each component orbital. Band calculations were also performed to

compare the UPS spectra with the calculated DOS and PDOSs. The results obtained in this study are summarized as follows:

(1) The UPS spectra showed a remarkable excitation energy dependence that was related to the photoionization cross sections of component atomic orbitals and the calculated DOS and PDOSs were consistent with the UPS spectra.
(2) Five bands were resolved in the valence band of LaCuOCh (Ch=S, Se, and Te), which were assigned from the VBM, to Ch p–Cu $3d$ antibonding band, Cu $3d$ nonbonding band, Ch p–Cu $3d$ bonding band, O $2p$–La $5d$ bonding band, and Ch $4p$–Cu $4s$, $3d$ bonding bands.
(3) The features of the valence-band structure were understood by means of the energy-band calculations and by the molecular-orbital diagrams of the $(La_2O_2)^{2+}$ and $(Cu_2Ch_2)^{2-}$ layers. The differences between LaCuOCh were primarily derived from the variations in the Ch p energy levels, which accompanied the changes in the degree of hybridization between the Ch p and Cu $3d$ states.

[1]M. Palazzi, C. R. Seances Acad. Sci., Ser. 2 **292**, 789 (1981).
[2]W. J. Zhu and P. H. Hor, J. Solid State Chem. **130**, 319 (1997).
[3]J. E. Iglesias, K. E. Pachali, and H. Steinfink, Mater. Res. Bull. **7**, 1247 (1972).
[4]W. J. Zhu, Y. Z. Huang, F. Wu, C. Dong, H. Chen, and Z. X. Zhao, Mater. Res. Bull. **29**, 505 (1994).
[5]J. C. W. Folmer and F. J. Jellinek, J. Less-Common Met. **76**, 153 (1980).
[6]S. Hirose, K. Ueda, H. Kawazoe, and H. Hosono, Chem. Mater. **14**, 1037 (2002).
[7]A. Ouammou, M. Mouallem-Bahout, O. Peña, J.-F. Halet, J.-Y. Saillard, and C. Carel, J. Solid State Chem. **117**, 73 (1995).
[8]G. V. Vajenine and R. Hoffmann, Inorg. Chem. **35**, 451 (1995).
[9]C.-H. Park, D. A. Keszler, H. Yanagi, and J. Tate, Thin Solid Films **445**, 288 (2003).
[10]C. Zheng and R. Hoffmann, J. Am. Chem. Soc. **108**, 3078 (1986); R. Hoffman and C. Zheng, J. Phys. Chem. **89**, 4175 (1985).
[11]K. Ueda, S. Inoue, S. Hirose, H. Kawazoe, and H. Hosono, Appl. Phys. Lett. **77**, 2701 (2000); K. Ueda, S. Inoue, H. Hosono, N. Sarukura, and H. Hirano, Appl. Phys. Lett. **78**, 2333 (2001); K. Ueda and H. Hosono, J. Appl. Phys. **91**, 4768 (2002); H. Hiramatsu, K. Ueda, H. Ohta, M. Hirano, T. Kamiya, and H. Hosono, Appl. Phys. Lett. **82**, 1048 (2003).
[12]K. Ueda, H. Hiramatsu, H. Ohta, M. Hirano, T. Kamiya, and H. Hosono, Phys. Rev. B **69**, 155305 (2004).
[13]H. Hiramatsu, K. Ueda, H. Ohta, M. Orita, M. Hirano, and H. Hosono, Appl. Phys. Lett. **81**, 598 (2002); H. Hiramatsu *et al.*, Appl. Phys. Lett. **81**, 598 (2002); H. Hiramatsu, H. Kamioka, K. Ueda, M. Hirano, and H. Hosono, J. Ceram. Soc. Jpn. **113**, 10 (2005).
[14]H. Hiramatsu, K. Ueda, T. Kamiya, H. Ohta, M. Hirano, and H. Hosono, J. Phys. Chem. B **108**, 17344 (2004).
[15]S. Inoue, K. Ueda, H. Hosono, and N. Hamada, Phys. Rev. B **64**, 245211 (2001).
[16]K. Ueda, K. Takafuji, H. Hiramatsu, H. Ohta, T. Kamiya, M. Hirano, and H. Hosono, Chem. Mater. **15**, 3692 (2003).
[17]K. Ueda, H. Hosono, and N. Hamada, J. Phys.: Condens. Matter **16**, 5179 (2004).
[18]The bands *C* and *D* indexed in the previous study (Ref. 13) is newly assigned to band *C*/*D* and *E*, respectively, in this study.
[19]M. Usuda and N. Hamada, J. Phys. Soc. Jpn. **69**, 744 (2000).
[20]K. Ueda and H. Hosono, Thin Solid Films **411**, 115 (2002); K. Ueda, K. Takafuji, and H. Hosono, J. Solid State Chem. **170**, 182 (2003).
[21]B. A. Popovkin, A. M. Kusainova, V. A. Dolgikh, and L. G. Aksel'rud, Russ. J. Inorg. Chem. **43**, 1471 (1998).
[22]S. Hüfner, *Photoelectron Spectroscopy* (Springer, Berlin, Heidelberg, 1995).
[23]J.-J. Yeh, *Atomic Calculation of Photoionization Cross-Sections and Asymmetry Parameters* (Gordon and Breach Science, Langhorne, PA, 1993).